Predicting Land Surface Temperature With Uncertainty Estimation Using a Community Sensor Network and Machine Learning

Tom Narock[1,*], Anna Kulikova[1], Sakib Hussein[1], Marcellus Mwangi[1], and Abdul Siam[1]

[1] Department of Computer and Data Science, Goucher College, 1021 Dulaney Valley Rd, Baltimore, MD 21204, USA

* **Correspondence:** Thomas.Narock@goucher.edu

Abstract: Urban Heat Islands (UHIs) are areas in cities that experience higher temperatures than surrounding areas due to construction features such as buildings, roads, and a general lack of vegetation. UHIs, which pose a threat to public health while also increasing energy usage, are often defined using land surface temperatures. Our study demonstrates how a community sensor network from the Baltimore Social-Environmental Collaborative (BSEC) can be paired with advances in machine learning to provide near real-time predictions of UHIs with uncertainty estimates. While prior research has investigated the use of neural networks in UHI assessment, those efforts did not include uncertainty quantification. We demonstrate how uncertainty quantification can be incorporated into UHI prediction in Baltimore, Maryland. We show how a machine learning approach using community weather stations compares to ground-truth values from Landsat 9 spacecraft measurements in summer 2023. Moreover, we show how the capturing of different types of uncertainty are informative for future smart city planning. This information can empower city planners and residents to proactively address the risks associated with UHIs, potentially reducing heat-related illnesses.

Keywords: Neural Networks, Bayesian Neural Networks, Uncertainty Quantification, Land Surface Temperature, Smart Cities, Urban Heat Islands

1. Introduction

Urban areas cover only 3% of the Earth's land surface [7]; yet, half of the world's population resides in urban areas [26]. Residency in urban areas is estimated to increase to 70% by 2050. The population needs of urban residency have led to more infrastructure development resulting in urban morphology changes and increased anthropogenic heat released into the atmosphere. Conventional human-made materials such as pavements and roofing tend to absorb and emit more of the sun's heat compared to trees, vegetation, and other natural surfaces. Additional complications arise in heavily developed areas where surfaces and structures obstructed by neighboring buildings become unable to release their heat readily. Cities with narrow streets and tall buildings become urban canyons blocking natural wind flow that would bring cooling effects. The result is a so-called Urban Heat Island (UHI) in which urban areas experience higher temperatures than surrounding suburban and rural areas. Often, heat islands build throughout the day and become more pronounced after sunset due to the slow release of heat from urban materials.

There are four primary public health impacts related to UHIs.

1.) Increased Energy Consumption - heat islands increase electricity demand for air conditioning. Increases in demand of 9% for each 2° F increase in temperature have been observed in the United States [12]. This leads to substantial energy expenses as the most intense UHIs can be 20° F hotter than nearby rural areas.
2.) Elevated Emissions of Air Pollutants - meeting the increased electricity needs often leads utility companies to use more fossil fuels, the output of which can be pollutants that are harmful to human health.
3.) Compromised Human Health - heat can exacerbate respiratory conditions such as asthma. In Baltimore City where our study was conducted, youth asthma rates are the highest anywhere in the state of Maryland with Baltimore also having the state's highest number of emergency department visits for asthma-related health issues [5]. While a number of factors contribute to a higher prevalence of asthma in Baltimore, studies have shown high temperatures can worsen air quality by facilitating the formation of ground-level ozone, a major asthma trigger. The Environmental Integrity Project, has shown a strong connection between Baltimore City asthma rates and toxic air [9].
4.) Impaired Water Quality - the high temperatures of pavement and rooftop surfaces can heat stormwater runoff, which subsequently raises water temperatures in streams, rivers, and ponds. Temperature surges in urban streams as much as 18° F due to heated runoff and has been shown to be deadly for aquatic life [30].

The United States Environmental Protection Agency defines[1] two types of UHIs. A Surface Urban Heat Island (SUHI) forms due to the aforementioned roadways and rooftops absorbing and emitting heat to a greater extent than most natural surfaces. Conventional roofing materials can be 66° F warmer than the surrounding air temperature [6]. This type of heat island tends to be most intense during the day when the sun is shining. Alternatively, an Atmospheric Urban Heat Island (AUHI) forms from air being warmer in urban areas compared to outlying areas. Atmospheric heat islands vary much less in intensity than surface heat islands. These differences in formation lead to differences in impacts, techniques used to identify and measure them, and to some degree the methods available to mitigate them. For example, air temperatures (AUHIs) reflect the conditions experienced by people and are therefore useful in understanding public health risks. Surface temperatures, on the other hand, represent the heat energy given off by land, buildings, and other urban surfaces. This information can be particularly relevant for informing strategies to mitigate heat islands as SUHIs have a more localized effect and contribute to AUHIs by heating the surrounding air.

The differences in SUHIs and AUHIs lead to vastly different data sources being needed to identify them. Surface Urban Heat Islands are typically found using remote sensing data. Satellite measures (e.g. Landsat or MODIS) and used to calculate land surface temperature (LST), which refers to the temperature of the Earth's ground surface and is distinct from the air temperature reported in weather forecasts. LST is primarily influenced by factors like vegetation cover, soil moisture, and albedo, and is crucial for studying land-atmosphere interactions and climate analysis. LST is typically measured using satellite imagery, which can capture the thermal radiation emitted

[1] https://epa.gov/heatislands/what-are-heat-islands#characteristics

from the land surface. Unlike air temperature, LST varies significantly depending on the type of surface (grass, concrete, water) being observed and can heat up or cool down much faster than the surrounding air. Conversely, Atmospheric Urban Heat Islands are typically identified from weather stations and commonly available variables such as temperature, humidity, and wind speed.

We demonstrate in this study how a community network of weather stations from the Baltimore Social-Environmental Collaborative (BSEC) can be paired with advances in machine learning to provide near real-time predictions of LST with uncertainty estimates. These predictions, when combined with the sensors' initial purpose, weather data, can enable estimates of both SUHIs and AUHIs. Obtaining LST from weather data is highly desirable for continuous assessment of UHIs. Spacecraft orbits limit how frequently they can measure a given location. Even when a spacecraft is overhead, local weather can prohibit LST measurement. Predicting LST from more readily available weather data alleviates these challenges. While prior research has investigated the use of neural networks in UHI assessment, those efforts did not include uncertainty quantification. We demonstrate how Bayesian statistical approaches can be incorporated into neural networks enabling LST predictions with uncertainty estimates for Baltimore, Maryland during summer 2023. We compare the neural network predictions to ground-truth values of LST from the Landsat 9 spacecraft. Moreover, we discuss different types of uncertainty and show how capturing multiple types of uncertainty are informative for future smart city planning.

Our work is organized as follows. We next introduce related research discussing previous machine learning approaches to UHI prediction and also introduce the notion of Bayesian Neural Networks for uncertainty estimation. Section two introduces the BSEC network and the datasets used in our research while also detailing our methodology and neural network training. Section three presents results from the testing and evaluation of our neural network. Section four is our concluding section in which we discuss the implications of our results and next steps in our research.

Although several analytical modelling approaches for urban heat islands exist [19], the physical complexity of the phenomenon, the extensive urban details required to attain an accurate model and the increased computational time and costs have led researchers to the exploration of other prediction methods. One alternative prediction method is the neural network, which has a long history in urban heat island prediction studies (e.g. [23][18][11]). The relationship between landscape metrics and LST is complex and multifaceted. Acknowledging this, several studies have explored the relationship between various input features and output LST predictions. Some of the these studies utilized machine learning approaches while in other cases the identified relationships were leveraged in subsequent machine learning studies (e.g. [3][8][13][14][16]). In an example of the latter scenario, [25] have shown how morphology features impact LST predictions in neural networks. This research has significantly enhanced UHI prediction methods. However, this prior research is focused on point estimate predictions of LST. Recent advances in neural networks, namely Bayesian Neural Networks (BNN), allow for uncertainty quantification in addition to their predictions.

Traditional neural networks optimize a loss function, typically through gradient descent, to obtain optimal weight values, which work as a function approximator mapping input feature values to output predictions. A BNN, by contrast, does not seek fixed model parameters. In a BNN [29] the network weights and output predictions are all probability distributions. Passing the same input

through the trained network will result in different predictions as different weights are sampled from the distributions on each pass. This allows a BNN to effectively work as an ensemble with the variability in predictions for each input enabling uncertainty quantification. There are two main types of uncertainty one can model [15]. Aleatoric uncertainty captures noise inherent in the observations and is reflected in the output prediction being a probability distribution. Epistemic uncertainty accounts for uncertainty in the model parameters, which, in a machine learning context, captures our ignorance surrounding the optimal neural network weights. Epistemic uncertainty can be reduced given enough data, as more training data leads to better refinement of model parameters. Aleatoric uncertainty, on the other hand, captures noise inherent in the observations and is irreducible. We create a Bayesian neural network capable of capturing both aleatoric and epistemic uncertainty. Aleatoric uncertainty is modeled by placing a probability distribution over the model's output. Similarly, epistemic uncertainty is modeled by replacing neural network weights, which are traditionally point estimates, with probability distributions. In this work, we use normal distributions for all uncertainty modeling. A graphical comparison of traditional neural networks and Bayesian neural networks is shown in Figure 1.

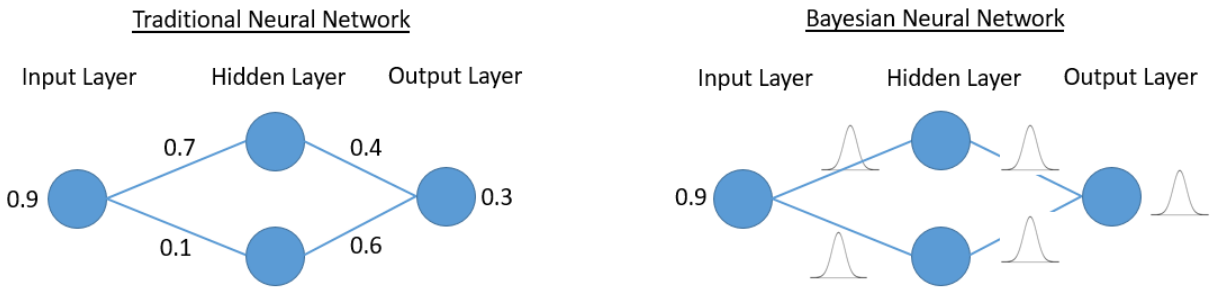

Figure 1. Graphical comparison of traditional and Bayesian Neural Networks. The former use point estimates while the latter sample from distributions.

Aspects of Bayesian machine learning have made their way to UHI prediction. [1] used a Bayesian network to classify UHI intensity in New Jersey. A second study by the same authors [2] explores network pruning and investigates causal linkages among factors impacting UHI severity. [10] provide a comprehensive review of machine learning in UHI prediction, including the recent Bayesian approaches.

While [1] and [2] use a Bayesian network, it is a Delphi-based approach and not the neural network approach currently being explored in other domains (see for example, [21] and [22]). As such, it does not capture both aleatoric and epistemic uncertainty. In this work, we introduce a novel BNN capable of capturing both types of uncertainty. Rather than predict UHI intensity categorically, as was done in [1], we use a regression approach to predict numerical LST values with uncertainty. This allows for flexibility in how those LST predictions, and their uncertainties, can subsequently be used to assess UHIs. Moreover, the inputs to our Bayesian neural network come from a network of weather stations with uneven spatial coverage of Baltimore City. We are able to further explore the impact distance has on prediction uncertainty and explore how BNNs

could assist in the optimal placement of sensors.

2. Methods and data sources

The Baltimore Social-Environmental Collaborative[2] (BSEC) contributes to climate action plans for Baltimore with a focus on improving the well-being of those who live in historically underserved neighborhoods. The BSEC mission involves co-designing climate solutions that respond to community concerns. BSEC scientists work in close partnership with Baltimore residents and a portion of their efforts involves deploying sensors in and around local communities. Observations at the city and neighborhood scales are used to understand issues related to urban heat islands, urban flooding, and air pollution.

BSEC had 23 weather stations deployed around Baltimore at the time of our study [28]. These weather stations were deployed in coordination with local communities and reside at a variety of locations including churches, vacant lots, private residences, public parks, and libraries. Two different types of weather stations are used - Ambient Weather stations and OttHydro stations. For consistency of measurements, we limit our study to Ambient Weather stations[3], which are much more plentiful, and also confine our study to stations within Baltimore City. The spatial distribution of these stations is shown in Figure 2. Each Ambient Weather station produces 27 measurements per hour, which are described in Table 1. We add two additional measurements, the Normalized Difference Vegetation Index used to approximate land cover/usage and the distance from the point of interest to the nearest BSEC Ambient Weather station. Together, this set of 29 measurements are the basis for the neural network input with the output being a probability distribution predicting the LST at the point of interest.

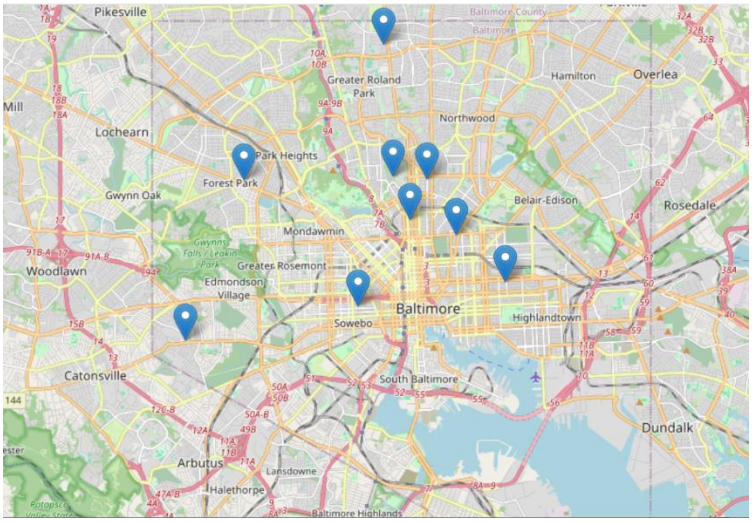

Figure 2. Spatial distribution of BSEC weather stations used in this study.

[2] https://bsec.21cc.jhu.edu/

[3] BSEC exclusively uses the ws-2902d model https://ambientweather.com/ws-2902-smart-weather-station

Table 1. Measurements That Form The Basis of The Neural Network Input.

Measurement	Data Source	Description
ndvi	USGS MRLC	Normalized Difference Vegetation Index used as approximate land cover/usage
bsecDistance	Computed during preprocessing	Distance in kilometers from the point of interest to the BSEC station whose data is being used
dewptHigh	BSEC weather station	Highest dew point temperature (deg C) recorded thus far in the day
dewptLow	BSEC weather station	Lowest dew point temperature (deg C) recorded thus far in the day
dewptAvg	BSEC weather station	Average dew point temperature (deg C) recorded thus far in the day
heatindexAvg	BSEC weather station	Average heat index temperature (the apparent temperature considering both the temperature and humidity) recorded thus far in the day (deg C)
heatindexHigh	BSEC weather station	Highest heat index temperature (the apparent temperature considering both the temperature and humidity) recorded thus far in the day (deg C)
heatindexLow	BSEC weather station	Lowest heat index temperature (the apparent temperature considering both the temperature and humidity) recorded thus far in the day (deg C)
humidityHigh	BSEC weather station	Highest relative humidity (%) recorded thus far in the day.
humidityLow	BSEC weather station	Lowest relative humidity (%) recorded thus far in the day.
humidityAvg	BSEC weather station	Average relative humidity (%) thus far in the day.
tempHigh	BSEC weather station	Highest air temperature (deg C) recorded thus far in the day
tempLow	BSEC weather station	Lowest air temperature (deg C) recorded thus far in the day
tempAvg	BSEC weather station	Average air temperature (deg C) recorded thus far in the day
pressureMax	BSEC weather station	Maximum surface pressure (hPa) recorded thus far in the day
pressureMin	BSEC weather station	Minimum surface pressure (hPa) recorded thus far in the day

pressureTrend	BSEC weather station	Change in surface pressure (hPa) since last recording
solarRadiationHigh	BSEC weather station	Highest incoming solar radiation (W/m^2) recorded thus far in the day
uvHigh	BSEC weather station	Highest radiation in the UV wavelength (W/m^2) recorded thus far in the day
winddirAvg	BSEC weather station	Average wind direction thus far in the day (degrees)
windchillAvg	BSEC weather station	Average wind chill temperature (the apparent temperature considering both the temperature and the wind speed) recorded thus far in the day (deg C)
windchillHigh	BSEC weather station	Highest wind chill temperature (the apparent temperature considering both the temperature and the wind speed) recorded thus far in the day (deg C)
windchillLow	BSEC weather station	Lowest wind chill temperature (the apparent temperature considering both the temperature and the wind speed) recorded thus far in the day (deg C)
windgustAvg	BSEC weather station	Average wind gust (m/s) thus far in the day. Gusts are reported when the peak wind speed reaches at least 16 knots and the variation in wind speed between the peaks and lulls is at least 9 knots.
windgustHigh	BSEC weather station	Highest wind gust (m/s) thus far in the day
windgustLow	BSEC weather station	Lowest wind gust (m/s) thus far in the day
windspeedAvg	BSEC weather station	Average wind speed (m/s) thus far in the day
windspeedHigh	BSEC weather station	Highest wind speed (m/s) thus far in the day
windspeedLow	BSEC weather station	Lowest wind speed (m/s) thus far in the day

Landsat 9 [17] measurements of Baltimore in summer 2023 were obtained from the United States Geological Survey's (USGS) EarthExplorer interface[4]. We restricted our search to days having less than 30% cloud cover to maximize coverage of the city. This resulted in four dates being available: 07/14/2023, 07/30/2023, 08/23/2023, and 08/31/2023. All Landsat 9 measurements of Baltimore occur at 15:46 GMT.

Landsat data were first preprocessed using the QA PIXEL variable, which is a quality assurance flag, to remove clouds, water, and pixels with missing data. We next filtered out Baltimore City using

[4] https://earthexplorer.usgs.gov/

latitude and longitude boundaries. LST was then computed using the algorithm of [4] via the Python pylandtemp library [20]. Landsat 9 has a spatial resolution of 30 meters, which resulted in roughly 230,000 LST measurements across Baltimore City per day. Although, this varied somewhat depending on cloud cover and pixel quality. BSEC data were also preprocessed using their quality control variable to filter out poor quality weather measurements. For each LST measurement, we obtained weather data one hour prior from the nearest BSEC weather station. We used Haversine distance to find the closest available BSEC weather station for each pixel in the Landsat images. We note that "closest available" implies geographic proximity and data availability. Occasionally, the closest BSEC weather station did not have usable data during the time of the LST measurement and the next closest BSEC station had to be used. Distances between LST measurements and BSEC weather stations were computed using the Haversine formula

$$\text{distance} = 2r \ \ arcsin\left(\sqrt{\frac{1-\cos(\Delta\varphi)+cos(\varphi_1)\cos(\varphi_2)(1-\cos(\Delta\lambda))}{2}} \right) \qquad (1)$$

where φ_1 and φ_2 are the latitudes of the LST measurement and BSEC weather station, respectively. λ represents the longitudes of the LST measurements and BSEC station with Δλ being the difference in longitude and $\Delta\varphi$ being the difference in latitude. We used a value of 6378 km for r, which represents the radius of the Earth. A histogram of all the distances between available BSEC weather stations and LST measurement is shown in Figure 3.

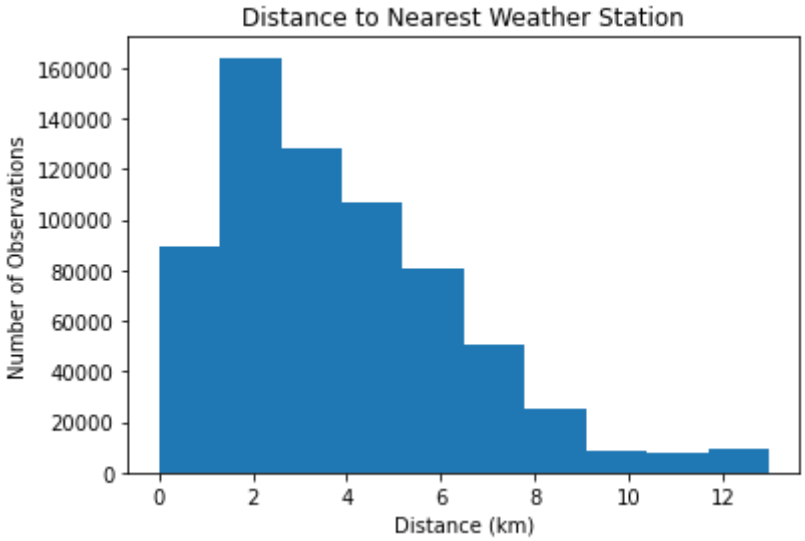

Figure 3. Histogram of distances between LST measurements and closest available BSEC weather station.

The median distance was 3.37 km and the largest distance was 12.9 km. Figure 4 shows the distribution of LST measurements occurring in our study. Our dataset had a mean LST of 73 degrees Fahrenheit and a standard deviation of 6.84 degrees Fahrenheit.

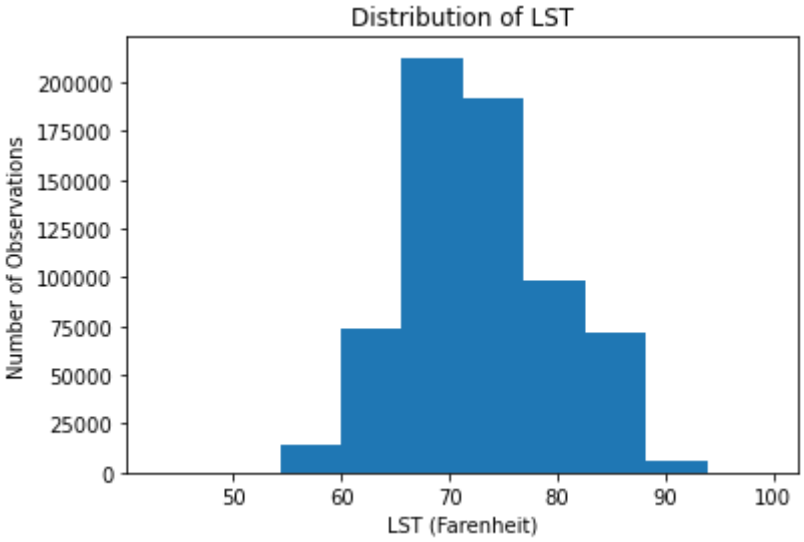

Figure 4. Distribution of LST measurements seen in this study.

When combined, the four days of data form a single machine learning ready dataset consisting of 669,309 measurements across the 29 variables described in Table 1. This dataset was then split into training and testing portions. Eighty percent of the data was used to train the neural network with the remaining twenty percent being reserved for testing and evaluation. We used a stratified train-test split to ensure the proportions of BSEC distances (Figure 2) were maintained in both the training and testing sets. In the end, 535,447 measurements from across Baltimore City were used to train the neural network and 133,862 measurements were withheld for subsequent testing and evaluation.

Principal Component Analysis (PCA) is a dimensionality reduction technique that transforms high-dimensional data into a lower-dimensional space while preserving the maximum amount of variance. It works by identifying orthogonal linear combinations of original features called principal components, where the first component captures the most variance in the data, the second component captures the next most variance orthogonal to the first, and so on. By selecting a subset of these principal components that explain a significant proportion of the data's variance we can reduce the number of input features, mitigate multicollinearity, and improve computational efficiency by reducing the size of the neural network. The process involves computing the covariance matrix, calculating eigenvectors and eigenvalues, and projecting the original data onto the new lower-dimensional space defined by these principal components. We applied PCA to address multicollinearity between BSEC weather parameters and also to reduce the complexity of our neural network. We selected a subset of principal components that retained 95% of the variance, which resulted in a reduction of neural network inputs from 29 to 7.

Our BNN consists of 4 layers: an input layer, two hidden layers, and an output layer. The input layer takes the 7 principal components from PCA analysis. The hidden layers consisted of 14 and 7 nodes, respectively, and the output layer predicts the mean and variance of a normal distribution for the LST at the input location. This resulted in 12,126 trainable parameters. The neural network was trained for 200 epochs with a batch size of 256. The 133,862 measurements of the test set were then used to evaluate the trained network. We made 100 predictions for each measurement in the test set.

The output of the BNN is a probability distribution; thus, every LST prediction included a mean and variance for the predicted normal distribution. Aleatoric uncertainty was then computed as the mean of the 100 variances and epistemic uncertainty as the variance of the means, following [27]. Final predictions are computed as:

$$\mu_{final} = \frac{1}{N}\sum_{i=1}^{N}\mu_i \quad (2)$$

and

$$\sigma^2_{final} = \text{Aleatoric Uncertainty} + \text{Epistemic Uncertainty} \quad (3)$$

where

$$\text{Aleatoric Uncertainty} = \frac{1}{N}\sum_{i=1}^{N}\sigma_i^2 \quad (4)$$

where σ_i^2 is the variance of the ith prediction

$$\text{Epistemic Uncertainty} = \frac{1}{N}\sum_{i=1}^{N}(\mu_i - \mu)^2 \quad (5)$$

where μ_i is the ith predicted mean and μ is the overall mean of the means

The final predictions for mean and variance at each location are then used to generate credible intervals, which can be a more useful way of leveraging the probability distributions output by a BNN. A credible interval is a range of values that represents a certain level of probability that the true value of a parameter lies within that range. It's a specific section of the probability distribution where we have a specified degree of confidence that the true value resides. Credible intervals are the Bayesian analog to confidence intervals. We constructed 95% credible intervals indicating that we are 95% confident that the LST at that location is within the interval. We note that credible intervals are not unique as any given probability distribution has an infinite number of credible intervals of probability 0.95. We use the highest density interval, which is defined as the smallest interval that contains the desired probability. Example predictions are given in Table 2 and all of our highest density credible intervals are summarized in a histogram and discussed in the next section.

Table 2. Sample output for three locations in Baltimore

Prediction Location (Lat/Lon)	Mean of LST Prediction Distribution	Variance of LST Prediction Distribution	95% High Density Credible Interval	Actual LST (Celsius)	Epistemic Uncertainty	Aleatoric Uncertainty
(39.25, -76.62)	20.45	4.74	[16.36, 24.84]	21.12	0.08	4.66
(39.33, -76.58)	27.46	2.34	[24.53, 30.49]	25.90	0.08	2.26
(39.37, -76.59)	26.47	2.05	[23.67, 29.07]	27.32	0.02	2.04

3. Results

Figure 5 shows the actual LST versus the predicted LST and Figure 6 shows a histogram of the residual LST (predicted minus actual).

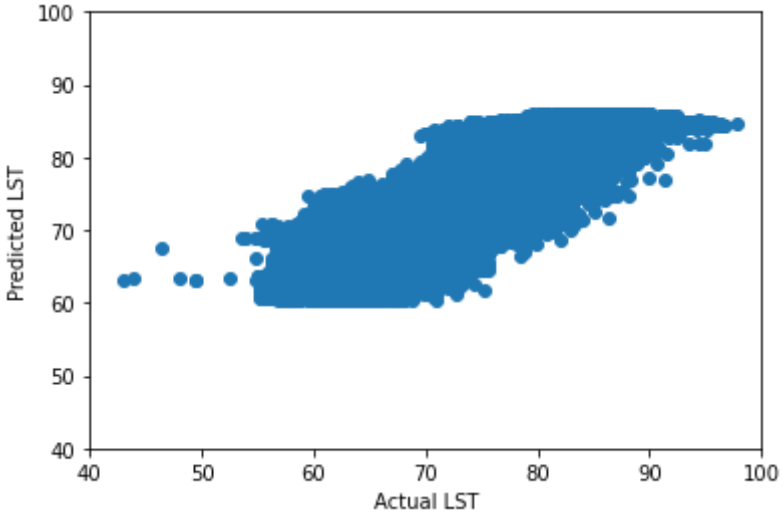

Figure 5. Actual vs predicted LST.

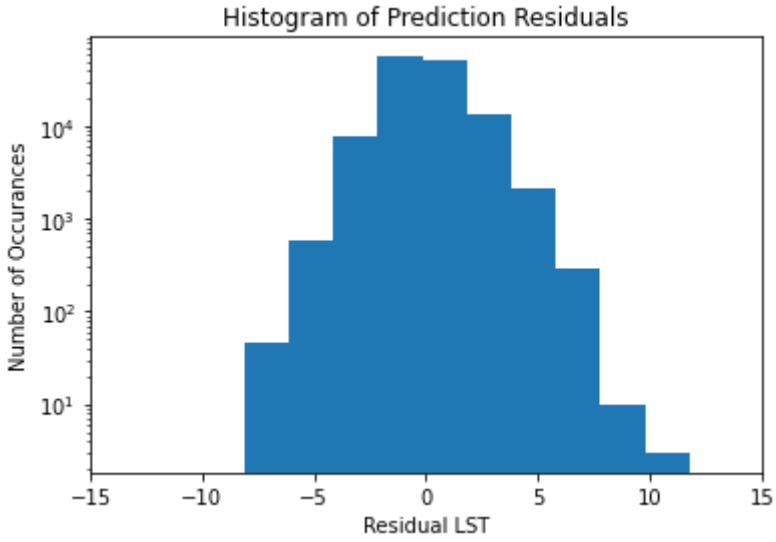

Figure 6. Histogram of Bayesian Neural Network prediction residuals (predicted – actual).

We obtained a mean absolute error (MAE) of 1.21 degrees. As shown in Figure 6, most predictions are within +/- 5 degrees of the actual LST; although, some locations differ by 10 degrees or more. Figure 7 shows the spatial distribution of residuals.

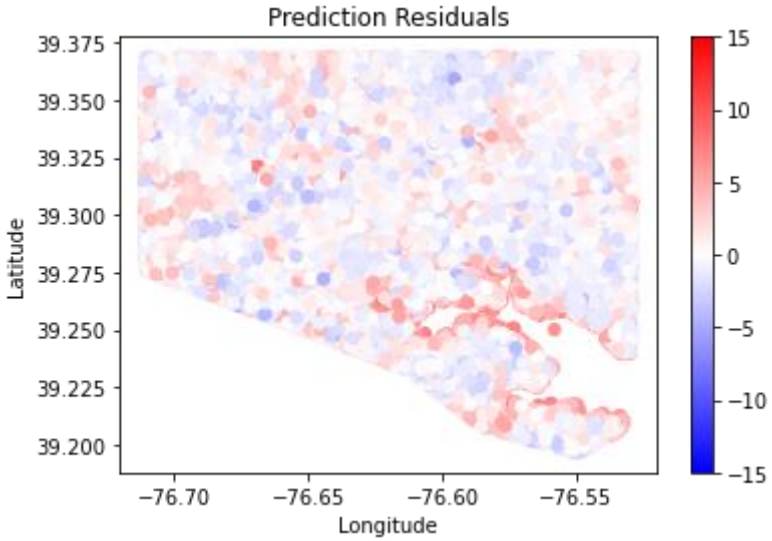

Figure 7. Spatial distribution of prediction residuals (predicted – actual value).

One of the major benefits of a Bayesian neural network is the additional ability to quantify uncertainty. In our application, aleatoric uncertainty represents the inherent variability in LST at each location and the difficulty predicting LST with certain urban morphologies. It arises from the unpredictable nature of the phenomenon being studied and theoretically cannot be reduced by gathering more data. Epistemic uncertainty represents the model's uncertainty about making an LST prediction given a combination of input features and is typically related to lack of, or limited number of, observations. The combination of these two types of uncertainty can

provide insights to the users of the neural network and the maintainers of the sensor network. For example, high aleatoric and low epistemic uncertainty at a particular location would indicate the neural network is confident that location exhibits naturally high variability in LST. Conversely, low aleatoric and high epistemic uncertainty at a location would indicate the neural network has low confidence in even making a prediction at this location (possibly due to limited observations of that location during training). The spatial distributions of aleatoric and epistemic uncertainty are shown in Figure 8 along with the land use characteristics of Baltimore City. Land use data are from the Multi-Resolution Land Characteristics Consortium Viewer[5] of the USGS.

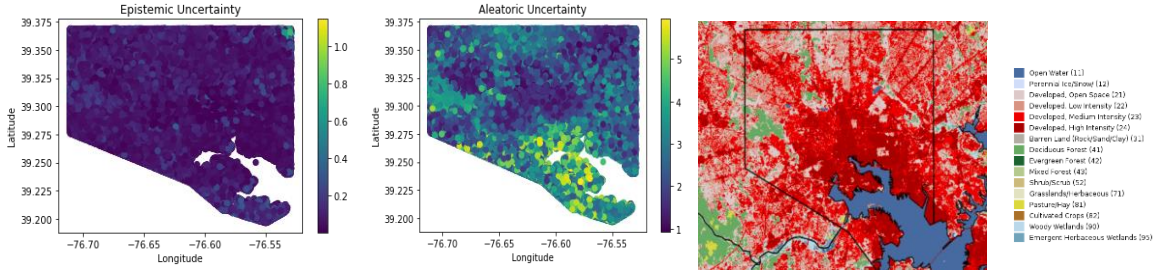

Figure 8. Spatial distribution of uncertainty alongside land use characteristics.

From Figure 8, we can see that the largest aleatoric uncertainties occur in southern Baltimore where there is a combination of highly developed area and harbor. We also see patches of higher aleatoric uncertainty in western Baltimore in the area around deciduous forest. This is Leakin Park a 1,216 acre deciduous forest, which is one of the largest in the city. High epistemic uncertainty appears to be confined to the northeast corner of the city. Figure 9 shows a histogram of the 95% high density credible intervals produced from our predictions.

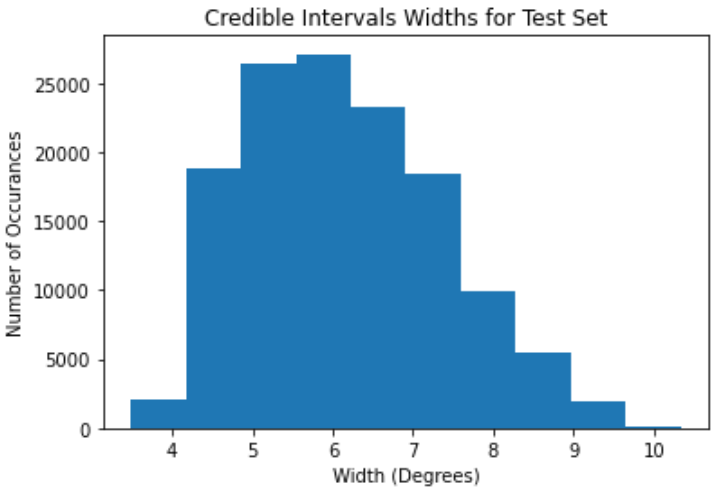

Figure 9. Distribution of 95% high-density credible intervals

[5] https://www.mrlc.gov/viewer/

As seen in Figure 9, the majority of our 133,862 test location produced 95% high density credible intervals with width between 5 and 7 degrees. In the most certain parts of Baltimore City the credible intervals had widths up to 10 degrees. We found that 95% of our 133,862 credible intervals contained the true LST value as expected. Yet, the number of credible intervals with wide widths was concerning. While aleatoric uncertainty is theoretically irreducible uncertainty inherent in the data, in practice its estimation through BNNs is subject to epistemic uncertainty. The neural network is learning to estimate both the actual data uncertainty (true aleatoric) and its confidence in that uncertainty estimate (epistemic). A common approach to train BNNs, and the one used here initially, is to use negative-log likelihood (NLL). [24] have shown this approach can "hide" epistemic uncertainty by inflating aleatoric uncertainty estimates (through larger predicted variances) because it's often easier for the network to increase predicted variance than to accurately model uncertainty in its parameters. The neural network might not be able to distinguish between true data noise and its own uncertainty about the data noise. In other words, the BNN can be confident in its predictions (low epistemic uncertainty) if it simply gives its predicted distributions high variance (leading to high aleatoric uncertainty). A prevalence of wide credible intervals (Figure 9) and general low epistemic uncertainty suggests the high aleatoric uncertainty we are seeing might be partially epistemic uncertainty being misattributed through the training process. [24] proposed a means of testing for this via beta-NLL. They introduce a beta term into negative-log likelihood, which penalizes the neural network for minimizing epistemic uncertainty at the expense of large variances. We note that beta-NLL is not reducing the true aleatoric uncertainty, but rather potentially getting closer to the true aleatoric uncertainty by discouraging the network from using inflated variance estimates as a "catch-all" for uncertainty and forcing the network to better separate what uncertainty comes from data noise versus model uncertainty.

The beta-nll approach uses a beta value between 0 and 1 with smaller values imparting more penalty. When beta equals one the beta-NLL and NLL approaches are equivalent. We tested our BNN with beta-NLL and values of 0.1, 0.5, and 0.75. We did not find any significant reduction in aleatoric uncertainty. This result suggests that most of the high aleatoric uncertainty is physically justified and not an artifact of neural network training. Particularly in the downtown harbor area, the high aleatoric uncertainty is likely a result of complex urban morphology such as the harbor-land interface, urban canyon effects, mixed surface materials, anthropogenic heat sources, and lack of BSEC weather stations nearby.

While the LST predictions themselves are useful for UHI assessment, the uncertainty maps can help BSEC and city planners optimize sensor deployment. The high aleatoric and low epistemic uncertainty in the harbor and western portions of the city is the BNN saying “We are confident there is high natural variability here". The high uncertainty isn't from model doubt but from genuine variability. It suggests additional sensors in this area could help characterize real variability. Conversely, in the northeast corner of the city we have higher epistemic uncertainty and low aleatoric uncertainty (Figure 8). In this location, the BNN gives narrow prediction intervals, but is acknowledging little confidence in those predictions. Additional sensors in this area could reduce epistemic uncertainty by providing more data. As a result, the aleatoric uncertainty might increase if the area turns out to be more naturally variable than the

BNN thinks. While instructive, uncertainty reduction is but one factor. Decisions regarding sensor deployment should also factor in environmental justice considerations, cost, and accessibility of locations.

An additional benefit of BNNs is their ability to flag so-called "out-of-distribution" data (OOD). OOD refers to data that significantly differs from the data used to train a machine learning model. OOD data leads to unreliable predictions because the neural network is not familiar with it having never seen anything similar during training. This is concerning for traditional neural networks as they have no mechanism to alert the user of the data being OOD. However, with a BNN, OOD data should result in epistemic uncertainty higher than what was seen during testing, enabling a mechanism for their potential detection. Although, the aforementioned practical challenges of the neural network attributing uncertainty to the data rather than to the model can complicate how OOD events are reflected in practice [15].

We simulated an extreme weather event to evaluate our BNN's ability to detect OOD inputs. Two locations were chosen, one in the downtown harbor area where aleatoric uncertainty is generally high and a second location in the northern part of the city where aleatoric uncertainty is amongst the lowest in the city. Air temperature measurements at these locations were artificially inflated by ten degrees before the collective weather data were input into the BNN. Figure 10 shows the impact of this OOD event on total uncertainty (aleatoric + epistemic). The red arrow in Figure 10 shows the northern location before the simulated extreme weather event (left panel) and during the event (right panel). We see a clear increase in total uncertainty. Used in this manner, a temporal history of uncertainty maps can help flag extreme weather events and alert communities that once reliable measurements are currently less reliable. Interestingly, in the harbor area where aleatoric uncertainty was already high, the simulated extreme weather raised epistemic uncertainty, but lowered aleatoric uncertainty. As a result, the harbor area extreme weather event was noticeable in epistemic uncertainty visualizations, but not in total uncertainty visualizations. These results suggest that a robust analysis of both types of uncertainty may be necessary to reliably identify extreme weather events.

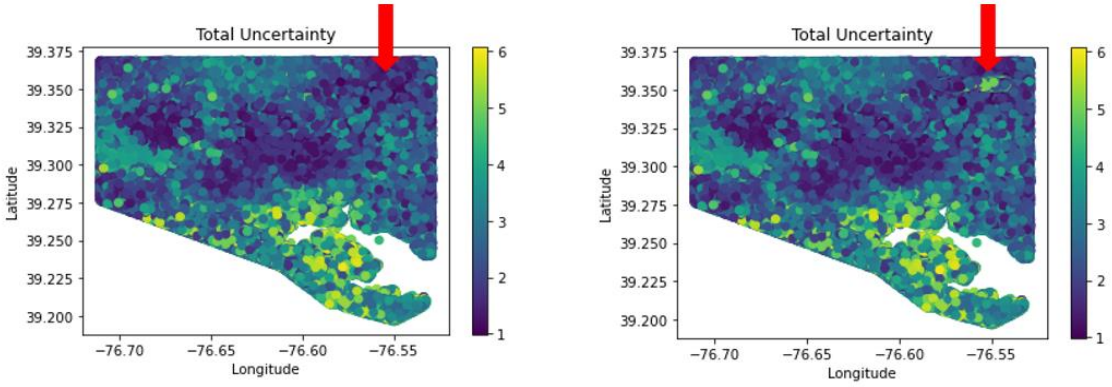

Figure 10. Impact of a simulated extreme weather event on uncertainty. The highlighted area (red arrow) sees an increase in uncertainty during the event signaling the current predictions may be unreliable.

4. Discussion and Conclusion

We have demonstrated how advances in neural network uncertainty quantification can be incorporated into UHI prediction in Baltimore, Maryland. Our approach leverages community weather stations and is able to predict land surface temperature with a mean absolute error of 1.21 degrees while also providing uncertainty intervals. Moreover, our work shows how capturing different types of uncertainty is informative for future smart city planning as it helps determine the location of future sensors and enables the flagging of extreme weather events.

Our work is not without limitations. The spatial context of urban morphology is important. Local LST is influenced by building density, adjacent land use types, and proximity to water and green spaces. Our neural network utilizes urban morphology at the location of the prediction only. We also note that our study took place during summer and did not include any days with precipitation. Future research will incorporate a broader context of nearby morphology and validate our methods in other cities where LST ground truth is available at different times of day and in different urban morphologies.

Despite these limitations, our research can serve as a novel example of the role uncertainty quantification, and specifically Bayesian neural networks, can play in urban planning, smart cities, and public health. Connecting local communities with sensors and machine learning can enable continuous LST assessment while empowering residents to proactively address the risks associated with a changing climate.

Acknowledgments

The authors are grateful for the Baltimore Social-Environmental Collaborative's (BSEC) free and open publishing of Baltimore weather data. We would also like to thank Dr. Darryn Waugh, Department of Earth & Planetary Sciences, Johns Hopkins University, for helpful discussions on BSEC instrumentation and deployment. Goucher College offers a Summer Research Program enabling undergraduate research opportunities. We are thankful for that program's financial and mentorship support to the coauthors of this paper.

Conflict of Interest

The authors declare they have no conflict of interest.

References

[1] Assaf, G., Rayan, X.I., and Assaad, H., (2023a), Predicting Urban Heat Island severity on the census-tract level using Bayesian networks, Sustainable Cities and Society, Volume 97, 2023, https://doi.org/10.1016/j.scs.2023.104756.

[2] Assaf, G., Hu, X., and Assaad, R.H., (2023b), Mining and modeling the direct and indirect causalities among factors affecting the Urban Heat Island severity using structural machine learned Bayesian networks. *Urban Clim.* 2023, *49*, 101570.

[3] Athukorala, D., & Murayama, Y. (2020). Spatial Variation of Land Use/Cover Composition and Impact on Surface Urban Heat Island in a Tropical Sub-Saharan City of Accra, Ghana. *Sustainability*, *12*(19), 7953. https://doi.org/10.3390/su12197953

[4] Avdan, U. and Jovanovska, G., 2016. Algorithm for Automated Mapping of Land Surface Temperature Using LANDSAT 8 Satellite Data, Journal of Sensors, 29 February 2016 https://doi.org/10.1155/2016/1480307

[5] Baltimore City Health Department, 2022, Chronic Disease Prevention, available online at: https://health.baltimorecity.gov/node/454

[6] Boujelbene, M., I. Boukholda, T. Guesmi, M.B Amara, and N. Khalilpoor. 2023. Solar reflection and effect of roof surfaces material characteristics in heat island mitigation: toward green building and urban sustainability in Ha'il, Saudi Arabia. *International Journal of Low-Carbon Technologies* 18:1039–1047.

[7] Center For International Earth Science Information Network (CIESIN) Columbia University, International Food Policy Research Institute-IFPRI, The World Bank, & Centro Internacional De Agricultura Tropical-CIAT. (2011). *Global Rural-Urban Mapping Project, Version 1 (GRUMPv1): Urban Extents Grid* (Version 1.00) [Data set]. Palisades, NY: NASA Socioeconomic Data and Applications Center (SEDAC). https://doi.org/10.7927/H4GH9FVG

[8] Connors, J.P., Galletti, C.S. & Chow, W.T.L. Landscape configuration and urban heat island effects: assessing the relationship between landscape characteristics and land surface temperature in Phoenix, Arizona. *Landscape Ecol* **28**, 271–283 (2013). https://doi.org/10.1007/s10980-012-9833-1

[9] EIP, Environmental Integrity Project, 2017, *Asthma and Air Pollution in Baltimore City,* report available online https://www.environmentalintegrity.org/wp-content/uploads/2017/12/Baltimore-Asthma.pdf

[10] Ghorbany, S., Hu, M., Yao, S., and Wang, C. (2024). Towards a Sustainable Urban Future: A Comprehensive Review of Urban Heat Island Research Technologies and Machine Learning Approaches. *Sustainability*, *16*(11), 4609. https://doi.org/10.3390/su16114609

[11] Gobakis, K, Kolokotsa, D., Synnefac, A., Saliari, M., Giannopoulouc, K., and Santamouris, M., (2011), Development of a model for urban heat island prediction using neural network techniques, Sustainable Cities and Society, 1, 2011, 104-115.

[12] Hibbard, K.A., F.M. Hoffman, D. Huntzinger, and T.O. West. 2017. Changes in land cover and terrestrial biogeochemistry. *In Climate Science Special Report: Fourth National Climate Assessment, Volume I* [Wuebbles, D.J., D.W. Fahey, K.A. Hibbard, D.J. Dokken, B.C. Stewart, and T.K. Maycock (eds.)]. U.S. Global Change Research Program, Washington, DC. pp. 277–302. doi: 10.7930/J0416V6X.

[13] Hou H. and Estoque, R.C., (2020), Detecting Cooling Effect of Landscape from Composition

and Configuration: An Urban Heat Island Study on Hangzhou, Urban Forestry & Urban Greening, Volume 53, 2020, https://doi.org/10.1016/j.ufug.2020.126719

[14] Kamarianakis, Y., Li, X., Turner, B.L. *et al.* On the effects of landscape configuration on summer diurnal temperatures in urban residential areas: application in Phoenix, AZ. *Front. Earth Sci.* **13**, 445–463 (2019). https://doi.org/10.1007/s11707-017-0678-4

[15] Kendall, A. and Gal, Y., (2017). What Uncertainties Do We Need in Bayesian Deep Learning for Computer Vision?, Proceedings of the 31st Conference on Neural Information Processing Systems (NIPS 2017), Long Beach, CA, USA. https://proceedings.neurips.cc/paper_files/paper/2017/file/2650d6089a6d640c5e85b2b88265dc2b-Paper.pdf

[16] Liu, Y., Peng, J., and Wang, Y., (2018), Efficiency of landscape metrics characterizing urban land surface temperature, Landscape and Urban Planning, Volume 180, 2018, pages 36-53, https://doi.org/10.1016/j.landurbplan.2018.08.006.

[17] Masek, J.G., Wulder, M.A., Markham, B., McCorkel, J., Crawford, C.J., Storey, J., Jenstrom, D.T., (2020), Landsat 9: Empowering open science and applications through continuity, Remote Sensing of Environment, Volume 248, 2020, 111968, ISSN 0034-4257, https://doi.org/10.1016/j.rse.2020.111968.

[18] Mihalakakou, M., Santamouris, N., & Papanikolaou, C. (2004). Cartalis simulation of the urban heat island phenomenon in Mediterranean climates. Pure and Applied Geophysics, 161, 429–451.

[19] Mirzaei, P. A., & Haghighat, F. (2010). Approaches to study urban heat island—Abilities and limitations. Building and Environment, 45(10), 2192–2201.

[20] Mudele, O., (2021). pylandtemp: A Python package for computing land surface temperature from Landsat satellite imagery. GitHub: https://github.com/pylandtemp/pylandtemp.

[21] Narock, T., Pal, S., Arsham, A. *et al.* Classifying Different Types of Solar-Wind Plasma with Uncertainty Estimations Using Machine Learning. *Sol Phys* **299**, 131 (2024). https://doi.org/10.1007/s11207-024-02379-8

[22] Ngartera, L., Issaka, M. A., & Nadarajah, S. (2024). Application of Bayesian Neural Networks in Healthcare: Three Case Studies. *Machine Learning and Knowledge Extraction*, *6*(4), 2639-2658. https://doi.org/10.3390/make6040127

[23] Santamouris, M., Mihalakakou, G., Papanikolaou, N., & Assimakopoulos, D. N.(1999). A neural network approach for modelling the heat island phenomenon in urban areas during the summer period. Geophysics Research Letters, 26(3), 337–340.

[24] Seitzer, M., Tavakoli, A., Antic, D., & Martius, G. (2022). On the Pitfalls of Heteroscedastic

Uncertainty Estimation with Probabilistic Neural Networks. *ArXiv, abs/2203.09168*.

[25] Tanoori, G., Soltani, A., Modiri, A., (2024), Machine Learning for Urban Heat Island (UHI) Analysis: Predicting Land Surface Temperature (LST) in Urban Environments, Urban Climate, Volume 55, 2024, https://doi.org/10.1016/j.uclim.2024.101962.

[26] United Nations, Department of Economic and Social Affairs, Population Division. (2018). World Urbanization Prospects: The 2018 Revision.

[27] M. Valdenegro-Toro and D. S. Mori, "A Deeper Look into Aleatoric and Epistemic Uncertainty Disentanglement," 2022 IEEE/CVF Conference on Computer Vision and Pattern Recognition Workshops (CVPRW), New Orleans, LA, USA, 2022, pp. 1508-1516, doi: 10.1109/CVPRW56347.2022.00157.

[28] Waugh, D., Lei, H., Collins, S., King, T., Montgomery, M., Różański, M., & the BSEC Team. (2024). Weather Data from BSEC Weather Stations (Version v2) [Data set]. MSD-LIVE Data Repository. https://doi.org/10.57931/2476281

[29] Wilson, A. G. and Izmailov, P. (2020) Bayesian Deep Learning and a Probabilistic Perspective of Generalization, 34th Conference on Neural Information Processing Systems (NeurIPS 2020), Vancouver, Canada https://proceedings.neurips.cc/paper/2020/file/322f62469c5e3c7dc3e58f5a4d1ea399-Paper.pdf

[30] Zahn, C., C. Welty, J.A. Smith, S.J. Kemp, M.L. Baeck, and E. Bou-Zeid. 2021. The Hydrological Urban Heat Island: Determinants of Acute and Chronic Heat Stress in Urban Streams. *Journal of the American Water Resources Association* 57(6): 941-955.

Supplementary

Data and code used in this study are available at: https://github.com/narock/lst_bnn

Narock, T., Kulikova, A., Hussein, S., Mwangi, M., & Siam, A. (2025). Land Surface Temperature Bayesian Neural Network (Version 1.0.0) [Computer software]. https://doi.org/10.5281/zenodo.14782915